CHEMICAL ENGINEERING TRANSACTIONS
VOL. 49, 2016
A publication of AIDIC
The Italian Association of Chemical Engineering
Online at www.aidic.it/cet
Guest Editors: Enrico Bardone, Marco Bravi, Tajalli Keshavarz

ISBN 978-88-95608-40-2; **ISSN** 2283-9216
DOI: 10.3303/CET1649017

Transport Regimes in Microfluidic Bioreactors: Hepatocyte Culture as a Case Study

Vincenzo Piemonte[a*], Luisa Di Paola[a], Stefano Cerbelli[b], Alberto Rainer[a], Marina Prisciandaro[c]

[a] Faculty of Engineering, University Campus Bio-Medico of Rome, via Alvaro delPortillo 21, 00128 Rome, Italy
[b] Dept. of Chemical Engineering, University of Rome "La Sapienza", via Eudossiana 18, 00184 Roma, Italy
[c] Dept of Industrial and Information Engineering and of Economics, University of L'Aquila, viale Giovanni Gronchi 18, 67100 L'Aquila, Italy
V.Piemonte@unicampus.it

Microflow reactors provide an ideal environment for the artificial growth of biological tissues, since temperature and concentration of the chemical species can be accurately controlled. In this work, we present an analysis of transport regimes and mechanisms underlying the cell activity in the microenvironment, in terms of reaction rates, product and reactants spatio-temporal profiles. We set up an advection-diffusion-reaction transport model to reproduce an hepatic sinusoide, to a design guidance for the experimental prototype.
The device consists of a U-shape sinusoid equipped with a microfluidic barrier, simulating endotelial cells, which separes the inflow-outflow channel for oxigen and nutrients uptake from internal chamber hosting hepatic cells. Due to the small scale, creeping flow conditions prevail, and the focus of the analysis to investigate the transport of oxygen and nutrients from the laminar streams crossing the device to the immobilized cell phase.
Assuming a nonlinear (Michaelis-Menten) kinetics of consumption of the transported species in the bulk cell phase, a wide variety of flow rate conditions are considered, as well as values of the bare molecular diffusivity of the transported species, ranging in an interval of four decades. In the specific scale and geometry, the impact of flowrate conditions on the concentration field is strongly dependent on the diffusivity of target chemical species.

Keywords: microfluidic, bioreactors, artificial organs, hepatocyte culture, Comsol.

1. Introduction

Microfluidic technologies allow a strict control of operating parameters in biological microsystems, providing high-density, high throughput arrays, so becoming an elective technology to scale-up biotechnological systems (Madia et al., 2009). A hot field of application deals with the development of *in vitro* devices mimicking the *in vivo* higher functions of cells and tissues, and physiological responses to different chemicals (Van Midwoud et al., 2009).
Additionally, microfluidic systems show an increased flexibility of experimental control, allowing fast changes of medium composition during experiments (van Widwoud et al., 2009).
The design of a cell culture microdevice relies on basic principles of chemical reactor design and cell biology: reaction kinetics, mass transfer, heat transfer, and (possibly) turbulence and mixing on product distribution, reactor productivity, size. These phenomena must be translated into accurate yet tractable models for device design and optimization (Vozzi et al., 2011).
Many works deal with microdevice design for cell culture, providing models that predict cell response to microenvironment conditions (Lee et al., 2005 and 2007; Zhang et al., 2007; Laganà and Raimondi,2012; Mazzei et al ., 2010; Van Midwoud et al., 2009; Powers et al., 2001; Rotemet al., 1992; Vozzi et al., 2011; Xia et al., 2009; Zahorodny-Burke et al., 2011). No one among the cited works integrates shear stress effects on cells and the concentration distribution of key species.

Please cite this article as: Piemonte V., Di Paola L. , Cerbelli S. , Rainer A., Prisciandaro M., 2016, Transport regimes in microfluidic bioreactors: hepatocyte culture as a case study, Chemical Engineering Transactions, 49, 97-102 DOI: 10.3303/CET1649017

In this work we fill this gap by analysing of transport regimes in microdevices through a dimensionless approach; the analysis is aimed at giving a synoptic characterization of the transport-reaction process for a wide variety of specific device geometries and operating conditions.
We applied the analysis in a first stage to an idealized linear device geometry, characterized by a counter-current flow configuration; we report results in terms of two dimensionless groups (*Pe* and *Th*), so to compare the diffusion, advection and reaction characteristic times.

2. Materials and Methods

2.1 Reactor geometry and dimensionless setting of the transport problem

Figure 1 depicts the scheme of the microfluidic chamber in the case of a linear geometry.

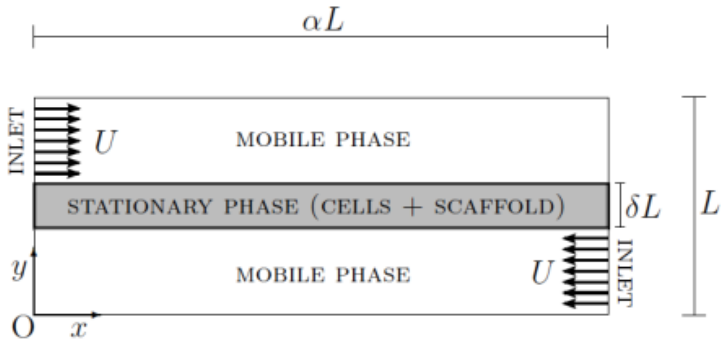

Figure 1. Microreactor geometry: uniform velocity and concentration profiles are assumed. As representative values of the geometric parameters: L_y = L = 1 mm , L_x = α L (α = 10), β = δL (δ = 0. 2). A flat velocity profile is assumed, v = v (y) = U (U = 100 μm s^{-1}).

Two inlet streams, supplying oxygen and nutrients to the immobilized cell phase, enter the in a counter-current configuration. The immobilized cell phase, comprising the scaffold and cells uniformly distributed, is assumed to possess a slab geometry of a specified thickness (*β*).
The steady-state mass balance for the mobile and stationary phases is:

$$0 = -v \cdot \nabla c_m + D\nabla^2 c_m \tag{1}$$

$$0 = D\nabla^2 c_s - R_m \cdot \frac{c_s}{K_m + c_s} \tag{2}$$

c_m and c_s are the nutrients concentration the mobile and the stationary phase, respectively; $\mathrm{v} = \big(\mathrm{u(x,y)}, \mathrm{v(x,y)}\big)$ is the laminar flow field in the mobile phase, D is the diffusivity coefficient in both phases; the reaction term in the stationary phase R_m follows a non linear, Michaelis-Menten kinetics.
The PDE boundary conditions are: uniform inlet concentrations in the mobile phase ($\mathrm{c_m} = \mathrm{c_0}$); null diffusive flux at the top and bottom walls of the device ($\mathbf{n} \cdot \nabla \mathrm{c_m} = 0$, **n** being a versor normal to the surfaces of interest); continuity conditions for the concentration and the local flux at the mobile/stationary phase boundary; Danckwerts' boundary conditions (pure convective flux) are imposed at the outlet cross-sections of the mobile phase).
The PDE system was made dimensionless as follows:

$$0 = -v \cdot \nabla \tilde{c}_m + \frac{1}{Pe}\nabla^2 \tilde{c}_m \tag{3}$$

$$0 = \nabla^2 \tilde{c}_s - Th \cdot \frac{\tilde{c}_s}{K_m^* + \tilde{c}_s} \tag{4}$$

in which $\tilde{c}_m = c_m/c_0$ and $\tilde{c}_s = c_s/c_0$ are the dimensionless concentrations in the mobile and stationary phase, respectively, $K_m^* = K_m/c_0$ is the dimensionless Michaelis-Menten constant, $Pe = UL/D$ is the Péclet number (in the mobile phase) and $Th = R_m \cdot L^2/(D \cdot c_{0)}$ is the Thiele number in the stationary phase.

3. Results

3.1 PDE solution and parametric analysis

The PDE problem was implemented in Comsol Multiphysics environment.

First of all, the velocity field in the mobile phase was derived. Assuming a water-like carrier fluid and the characteristic dimensions and velocity discussed in the previous Section, a Reynolds number of order 10^{-1} was obtained, suggesting prevailing laminar conditions. Figure 2 shows the developing laminar profile close to the entrance within one entrance length, $x_{max} = (1 - \delta)/2$.

The creeping flow solution was obtained setting a flat velocity profile at the entrance cross-section, a uniform pressure (with no viscous stresses) at the channel outlet, and no-slip conditions at the channel walls and at the boundary between mobile and stationary phase.

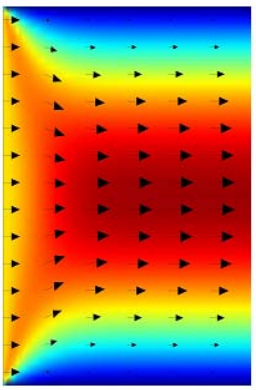

Figure 2. Development of the Poiseuille profile close to the device entrance in the mobile phase (within one entrance length, $x_{max} = (1 - \delta)/2$).

Therefore, we solved the scalar transport problem expressed by the dimensionless Eqs. (3)-(4): to avoid aliasing errors and inaccuracies due to interpolation, the same spatial discretization as the fluid-dynamic computation was used for the solution of the advection-diffusion-reaction problem.

Figure 3 reports the spatial (dimensionless) steady-state concentration fields at different Peclet values, (*Pe* = 10; 48) and at a fixed value of the Thiele modulus (*Th* = 48).

(a)

(b)

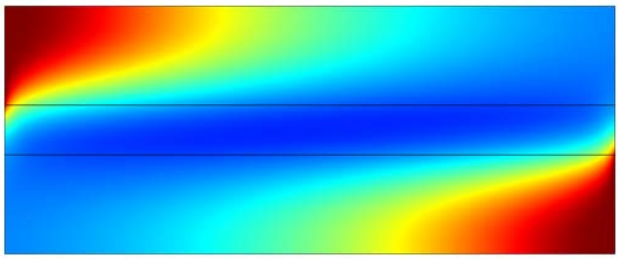

Figure 3 (a-b). steady-state dimensionless concentration profiles (Th = 48 and K_m^*=0.5) (a) Pe=10; (b) Pe=48.

Values of *Pe* and *Th* correspond to the characteristic velocity of *U* = 20 μm s^{-1} and *U* = 100 μm s^{-1}, respectively, matching with conditions that characterize transport and reaction of oxygen in artificial human tissues. At low *Pe* the concentrations in the mobile phase are very low, endangering the cell proliferation, so urging an advection-assisted feeding of oxygen and nutrients even at such tiny length-scales, as those associated with this choice of the dimensionless groups.
Figure 4 reports the concentration profiles along the vertical (Fig. 4a), and horizontal (Fig. 4b) axes of symmetry of the device. The transport parameters strongly affects the nutrient and oxygen supply, shifting from a condition of well-fed cells (low*Th* and high *Pe*, black lines) to the opposite scenario (gray lines in Figure 4 on the right).

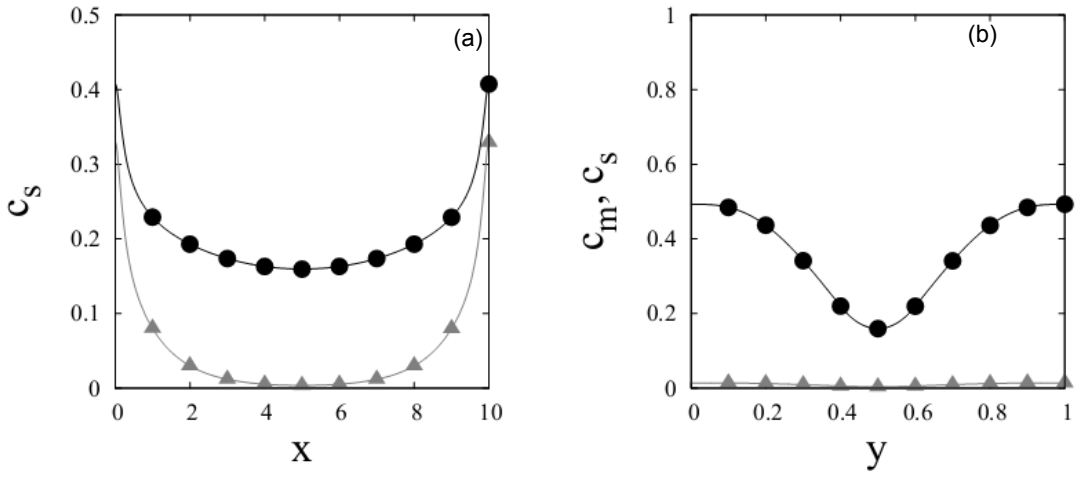

Figure 4 (a-b). Concentration profiles along the horizontal (a) and vertical (b) symmetry axes of the microflow bioreactor. Black line and bullets: Pe = 48. Gray line and triangles: Pe = 10.

These preliminary results markedly suggest that small changes of the transport parameters can have a strong impact on the environment where cells proliferate, and that an accurate design of the operating conditions based on the numerical solution of transport equations may support as an essential pre-requisite of a successful experimental campaign.
Next, we evaluated the influence of the two dimensionless groups *Pe* and *Th* on the average concentration $\langle c_s \rangle$ within the stationary phase Ω_s, defined as:

$$\langle c_s \rangle = \frac{1}{\mathrm{Vol}(\Omega_s)} \int c_s(x,y)\,dx\,dy \tag{5}$$

as well as on the dispersion of the concentration values about the average, quantified as a variance:

$$\langle \sigma_s \rangle = \frac{1}{\mathrm{Vol}(\Omega_s)} \int_{\Omega_s} (c_s(x,y) - \langle c_s \rangle)^2\,dx\,dy \tag{6}$$

Species diffusivity is being varied, while keeping all the other transport and operating parameters fixed. Thiele modulus was considered as an independent variable parameter and associated to Peclet number as $Pe = \left({Uc_0}/{R_{mL}}\right) \cdot Th = \gamma \cdot Th.$

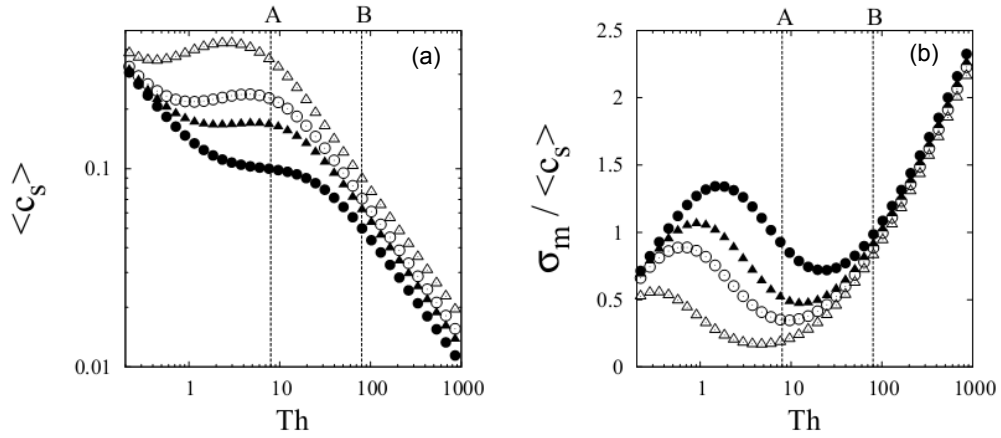

Figure 5 (a-b). Dependence of the average concentration$\langle c_s \rangle$(a) and of the scaled variance$\sigma_s/\langle c_s \rangle$(b) on the Thiele modulus at different values of γ (Solid circles: γ = 2.3; Solid triangles: γ = 4; Empty circles: γ = 5.75; Empty triangles: γ = 11.5). Dotted line "A" corresponds to a typical Th value for oxygen in these systems, whereas line "B" corresponds to a Th value descriptive for larger molecules (e.g. glucose).

Figure 5a depicts the results of the dependence $\langle c_s \rangle$ vs. *Th*, for different values of the coefficient *γ*, depending on flowrate *U*. A first practical implication is thats for a fixed device geometry and characteristic kinetic rate, the impact of fluid dynamics on concentration fields strongly depends on diffusivity. As expected, at low values of the *Th* modulus (large diffusivity), the flowrate has practically no impact on the concentration field (prevailing advection contribution in the transport equation). On the other hand, at large *Th* values (low diffusivity), $\langle c_s \rangle$ run parallel to each other in the double logarithmic scale. The intermediate *Th* region (when *Th* varies in the range one to ten, typical of transport of small molecules*)* shows a pronounced response of $\langle c_s \rangle$ with respect to flowrate. Note that this *Th* range also corresponds to the largest (normalized) concentration variance within the immobilized phase (Figure 5b), provoking spatial inhomogeneities into regions where cell survival and proliferation become critical.

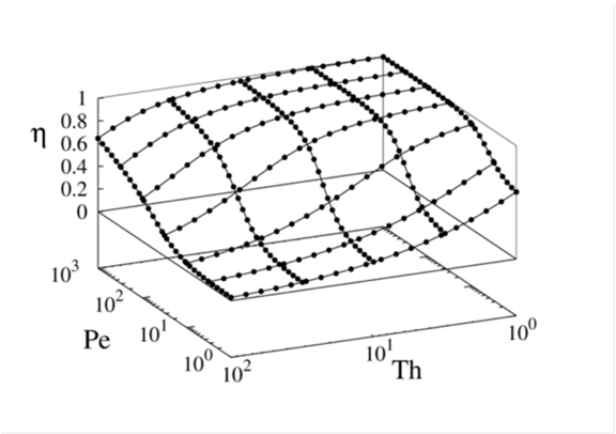

Figure 6. Overall reaction efficiency (η) for the linear counter-current geometry vs. the Peclet and Thiele parameters.

Figure 6 shows the overall reaction efficiency η, defined under the assumption of negligible characteristic time for transport compared to the reaction characteristic time. The low *Th* - large *Pe* region is characterized by a plateau, where the system response is essentially insensitive to variations of operating conditions. Conversely, the region of intermediate *Th* values displays a sharp transition of η in a quite small *Pe* interval. This sharp transition region can be used to test cell response to sudden environment changes by means of small flowrate variations.

4. Conclusion

This work reported a two-dimensional model for addressing transport of nutrients and oxygen to an immobilized cell phase in a microfluidic chamber, where species are fed by a laminar flow stream crossing the device. The dimensionless formulation of the advection-diffusion problem in the presence of Michaelis-Menten consumption kinetics for the immobilized cell phase allows to uncover different transport regimes when operating conditions are varied over a wide range parameter intervals. A wealth of steady-state solutions for a straight geometry configuration highlights ranges of the Peclet and Thiele numbers that should provide ideal environment for cell growth.

We find that the efficiency of species delivery to the immobile cell phase undergoes a sharp transition in a quite modest range of *Pe* and *Th*. While this condition should be avoided at the design stage of microbioreactors aimed at growing biological tissues, we suggested that operating in such critical conditions could be useful to understand cell response to environment variations, especially because the micro length-scales allow for swiftly passing from one operating condition to another.

It is noteworthing however, the present analysis does not take into account the biological aspects of cell maintenance, such as, *e.g.*, intercellular cell signaling, which may be crucial for a successful implementation of microfluidic-assisted growth of biological tissues in extracorporeal devices.

References

Lee P.J., Hung P.J., Lee1 L.P. 2007, An Articial Liver Sinusoid With a Microuidic Endothelial-Like Barrier for Primary Hepatocyte Culture, Biotechnol. Bioeng. 97, 1340-1346.

Lee P.J., Hung P.J., Rao V.M., Lee L.P. 2006, Nanoliter Scale Microbiore-actor Array for Quantitative Cell Biology, Biotechnol. Bioeng. 94 (1), 5-14.

Madia G., G. Barbieri, E. Drioli, Theoretical and experimental analysis of methane steam reforming in a membrane reactor, Can. J. Chem. Eng. 77 (1999) 698–706.

Powers M.J., Domandsky K., Kaazempur-Mofrad M.R.., Kalezi A., Capi-tano A., Upadhyaya A., Kurzawski P., Wack K.E., Stolz D.B., Kamm R.,

Rotem A., Toner M., Tompkins R.G., Yarmush M.L. 1992, Oxygen Uptake Rates in Cultured Rat Hepatocytes, Biotechnol. Bioeng. 40, 1286-1291.

van Midwoud P.M., Groothuis G.M.M., Merema M.T., Verpoorte E. 2009, Microuidic Biochip for the Perifusion of Precision-Cut Rat Liver Slices for Metabolism and Toxicology Studies, Biotechnol. Bioeng. 105, 184194.

Vozzi F., Mazzei D., Vinci B., Vozzi G., Sbrana T., Ricotti L., Forgione N., Ahluwalia1A. 2011, A Flexible Bioreactor System for Constructing In Vitro Tissue and Organ Models, Biotechnol. Bioeng. 108 (9), 2129-2140.

Zahorodny-Burke M., Nearingburg B., Elias A.L. 2011, Finite element anal-ysis of oxygen transport in microuidic cell culture devices with varying channel architectures, perfusionrates, and materials, Chem. Eng. Sci. 66, 62446253.

Zhang M.Y., Lee P.J., Hung P.J., Johnson T., Lee L.P., Mofrad M.R.K. 2007, Microfluidic environment for high density hepatocyte culture, Biomed Microdevices, 10, 117–121.